# Latest Developments in Gasoline Auto-Ignition Modelling Applied to an Optical CAI (Tm) Engine

V. Knop, S. Jay

*Oil & Gas Science and Technology – Rev. IFP*, Vol. 61 (2006), No. 1, pp. 121-137


Dossier

*Development and Control of Combustion Systems*
Évolutions et contrôle des systèmes de combustion

# Latest Developments in Gasoline Auto-Ignition Modelling Applied to an Optical CAI™ Engine

V. Knop[1] and S. Jay[1]

*1 Institut français du pétrole, 1 et 4, avenue de Bois-Préau, 92852 Rueil-Malmaison Cedex - France*
*e-mail: vincent.knop@ifp.fr - stephane.jay@ifp.fr*

**Résumé — Derniers développements en matière de modélisation de l'auto-inflammation essence appliqués à un moteur optique utilisant la combustion CAI™** — La prédictivité de la simulation d'un moteur fonctionnant en mode de combustion à allumage par compression dépend fortement de la qualité de la description du phénomène d'auto-inflammation. L'auto-inflammation contrôlée d'un mélange carburé à base d'essence (CAI™ pour Controlled Auto-Ignition) nécessite la prise en compte des spécificités chimiques du carburant dans des conditions de fonctionnement caractérisées par des basses températures et de faibles richesses. Les modèles existants, utilisant des corrélations, ne permettent pas de couvrir l'ensemble de ces situations ni la prise en compte d'hétérogénéités locales responsables du développement des sites d'auto-inflammation.

Ce papier décrit un nouveau modèle d'auto-inflammation basé sur l'exploitation de résultats de calculs de chimie complexe, opérés pour un large éventail d'indices d'octane et de taux de dilution par les gaz brûlés. Sur base des conditions thermodynamiques locales, la description du phénomène d'auto-inflammation est réalisée par interpolation dans une base de données regroupant la description des effets de flammes froides et celle de l'évolution de la combustion pour des carburants de référence (PRF pour Primary Reference Fuel). La validation de ce modèle est opérée en comparant les résultats de simulation 3D à ceux de calculs de chimie complexe pour des configurations homogènes ou des machines à compression rapide.

Un point de fonctionnement de référence, réalisé sur moteur à accès optique, est simulé afin de mettre en évidence les processus thermiques et chimiques responsables de l'apparition de l'auto-inflammation en combustion CAI™. Les résultats expérimentaux sont exploités pour évaluer la prédictivité du modèle en termes de valeurs moyennes, comme la pression cylindre, mais également pour les taux de réaction volumiques locaux comparés avec les visualisations directes de la lumière émise par les zones de combustion.

***Abstract — Latest Developments in Gasoline Auto-Ignition Modelling Applied to an Optical CAI™ Engine*** *— The accuracy of predictive engine modelling for Compression Ignition (CI) combustion modes is heavily depending on the quality of the description of the auto-ignition process. The Controlled Auto-Ignition (CAI™ ) combustion process is a CI combustion mode using gasoline as fuel. Its modelling requires to account for the chemical characteristics of the fuel in low temperature, low equivalence ratio operating conditions. Existing models based on correlations do not allow to cover the whole range of thermodynamic conditions encountered in those engines and the effect of local inhomogeneities on the auto-ignition occurrence.*

*A dedicated auto-ignition model derived from detailed chemical kinetics calculations for a wide range of burnt gas dilution ratios and octane numbers is presented in this paper. Depending on local thermodynamic conditions, 3D CFD auto-ignition parameters are interpolated in a database describing low temperature effects and progress variable reaction rates for Primary Reference Fuels (PRF). The model validation is performed by comparing 3D CFD calculations with detailed chemical kinetics results for homogeneous configurations and rapid compression machines.*

*To highlight the basic thermal and chemical processes responsible for the occurrence of auto-ignition in a CAI™ engine, a reference operating point for an optical diagnostic engine is simulated. The assessment of the quality of the model prediction relies not only on global data, such as mean in-cylinder pressure, but also on the comparison of local volumetric reaction rates with the direct visualisation of light emitted during engine operation.*

## NOMENCLATURE

### Latin

| | |
|---|---|
| $c$ | Progress variable (based on the consumed fuel) |
| $C_1$ | Fuel mass fraction consumed by the cool flame |
| $IO$ | Fuel Octane Number |
| $IO_x$ | $C_8H_{18}$ molar fraction for one mole of Primary Reference Fuel (PRF) |
| $T^u$ | Unburned gases temperature |
| $p$ | Pressure |
| $X_i$ | Molar fraction of species $i$ |
| $X_{res}$ | Residuals (inert gas) molar fraction |
| $Y_1$ | Intermediate species for the delay integration |
| $Y_{Fu}$ | Fuel mass concentration |
| $Y_{TFu}$ | Fuel tracer mass concentration |

### Greek

| | |
|---|---|
| $\phi$ | Global fuel/air equivalence ratio |
| $\tau_c$ | Chemistry characteristic time for the cool flame consumption |
| $\tau_{LT}$ | Cool flame auto-ignition delay |
| $\tau_{HT}$ | Main auto-ignition delay |
| $\omega_c$ | Progress variable reaction rate |
| $\omega_{ck}$ | Tabulated reaction rate |

## INTRODUCTION

Focussing on efficiency and limitation of harmful pollutant emissions, engine designers are looking for interesting alternatives beyond the continuously evolving conventional gasoline Spark Ignition (SI) and Diesel Compression Ignition (CI) combustions.

The main stream of development followed by research engineers is the combination of conventional SI or CI combustion at high loads with new concepts at low loads. A large part of these new concepts are commonly classified under the wide family of Homogeneous Charge Compression Ignition (HCCI) combustion allowing high efficiency and low pollutant emissions but unable to spread to high engine loads.

The main topics of HCCI combustion, both with gasoline or Diesel as fuel, is to create propitious conditions for auto-ignition in a highly diluted mixture. The very presence of an important amount of diluent is to control the conversion rate of the chemical energy located in the fuel into mechanical work while limiting parasitic effects that are heat transfer, pollutant formation or noise emission. Diluting fresh mixture leads to of a slow-down of chemical oxidation and to transfer a part of the heat released to the diluent.

The main benefits of slowing down combustion for part load operating points is to limit the instantaneous pressure gradient and related noise level, but also to decrease the local temperatures. The thermal capacitic effect of diluent is a further step towards lower local and global temperatures. Low temperatures are of utmost importance as heat transfer and pollutant formation depend on it. Indeed, a decrease in total heat transfer is a way to improve global combustion efficiency. Low temperatures allow to get very low NOx and soot emissions even if they may limit final oxidation of some intermediate combustion products like carbon monoxide.

Using gasoline as fuel, HCCI combustion may be obtained by three different ways, all insuring a sufficient mixture temperature near Top Dead Centre (TDC) to promote auto-ignition. The first one is compression ratio alteration. As a high compression ratio is certainly propitious for auto-ignition, it is an interesting way at part load but induces a main drawback at full load: it also promotes knock appearance. As engines are generally planned to use conventional SI combustion at high load, the solution is either a compromise about compression ratio allowing both combustions with sufficient efficiency or the creation of a Variable Compression Ratio (VCR) engine. The efficiency of such VCR engines has already been demonstrated [1-2] but includes costly developments and additional engine parts.

The second way is to use a mixture heater in the intake circuit based on an external heat source or an exchanger with exhaust gases [2-4]. This is efficient for steady state operating points but thermal inertia of the heating system is not compatible with transient operations.

Controlled Auto-Ignition (CAI™) uses burnt gases not only as diluent but also as an in-cylinder heat source [5-10]. This requires a precise control of the amount of burnt gases and of the mixture formation to control auto-ignition occurrence and timing. As a high amount of burnt gases from the preceding engine cycle is needed but as no major engine modification with respect to conventional engine is wanted, burnt gases have to be trapped using adapted valve lifts. Two types of valve lift strategies are known to be efficient: Negative Valve Overlap (NVO), which is direct in-cylinder burnt gas trapping, and Burnt Gas Re-Breathing (BGRB), which is based on burnt gas reaspiration during the intake process (see section "Valve actuation strategy" for more details).

## 1 DEVELOPMENT THROUGH COMBINED SIMULATION AND EXPERIMENT

Up to now, the CAI™ combustion process in four-stroke engines is limited to prototype engines due to the lack of precise comprehension of the physical phenomena that drive the auto-ignition occurrence and the subsequent combustion evolution. This lack of knowledge limits the engineers' ability to precisely control the auto-ignition timing and occurrence on a wide operating range without the use of specific laboratory devices.

To improve our knowledge about the CAI™ combustion process, the *IFP* research strategy is to combine 3D CFD calculation with optical diagnostic. The use of both of these means in an interactive way is expected to be an efficient way to rapidly progress.

The interaction between simulation and optical diagnostic is crucial. Indeed, numerous operating behaviours encountered with experimental tests are not fully understood and 3D CFD may be a source for more information. On the other hand, 3D CFD without any validation may quickly become a source for too optimistic results.

The use of 3D CFD to study CAI™ may be divided in two main parts: the simulation of the gas exchange process and the calculation of the auto-ignition and combustion processes. The simulation of the gas exchange process aims to better understand the influence of the adapted valve lift strategies on the in-cylinder mixing process and the resulting mixture homogeneity for species and/or local temperature. This type of 3D CFD calculation is not more difficult with CAI™ than with conventional SI or CI combustion and has already been reported at *IFP* and elsewhere [5, 7, 11].

The *predictive* calculation of the auto-ignition and combustion processes is a far more difficult task because this implies the development of a specific gasoline auto-ignition model. Such auto-ignition models have already been reported for knock appearance detection [12-14] but the application range of these models is limited to this particular phenomenon.

Based on *IFP*'s experience about auto-ignition modelling for Diesel engines both for conventional combustion and HCCI operation, the model used for gasoline auto-ignition in knocking conditions has been extended to CAI™ operating conditions.

## 2 3D CFD SOLVER AND GENERALISED COMBUSTION MODEL

### 2.1 IFP-C3D

The IFP-C3D code is a parallel hexahedral unstructured code developed at *IFP*. The Navier-Stokes equations are solved using a finite volume method extended with the Arbitrary Lagrangian Eulerian (ALE) method. The code uses the well-known time splitting decomposition. The temporal integration scheme is largely implicit. Concerning the liquid phase, evaporation and break-up using the Wave-FIPA model and spray – wall interaction are included. For turbulent combustion, the 3-Zone Extended Coherent Flame Model (ECFM3Z) developed at *IFP* is used. Species (and tracers), energy and the RNG k-ε turbulent diffusion terms are implicitly solved by a generic diffusion routine. Moreover, efficiently preconditioning the pressure matrix drastically reduces the simulation time. The convection terms are explicitly subcycled. A second order upwind scheme for scalar and momentum convection is used. The OpenMP paradigm has been chosen for parallelisation, as it is standardised, portable, scalable and adapted to modern super-scalar SMP machines. Overall, about 50% of the code is parallelised providing a very good and scalable speed-up (around 3 for 4 processors). Details and extensive validations of the code may be found in [15].

### 2.2 ECFM3Z

The principle of the ECFM3Z model is detailed in Figure 1. A complete description is available in [16] and the model is successfully applied to Diesel combustion in [17-18] and to gasoline combustion in [19-20]. Whereas other models use detailed kinetics directly or in a semi-reduced form [21], the ECFM3Z auto-ignition model uses pre-tabulated detailed chemistry computation results. In this part, we briefly summarise the ECFM3Z model which blends the ECFM and CFM3Z approaches into a unique combustion model.

In order to correctly represent the mixing regions, the ECFM3Z model includes a description of the local stratification (*Fig. 1*) by considering three regions of mixing: one region (region F) contains only pure fuel, the second region (region M) contains a mixture of fuel and air (plus possible additional EGR) and the third region (region A) contains fresh air (plus possible additional EGR). During injection, the evaporation of the spray droplets leads to a source of mass in region F. The fuel in region F begins to mix with the air (+EGR) of region A and they form the mixture region M.

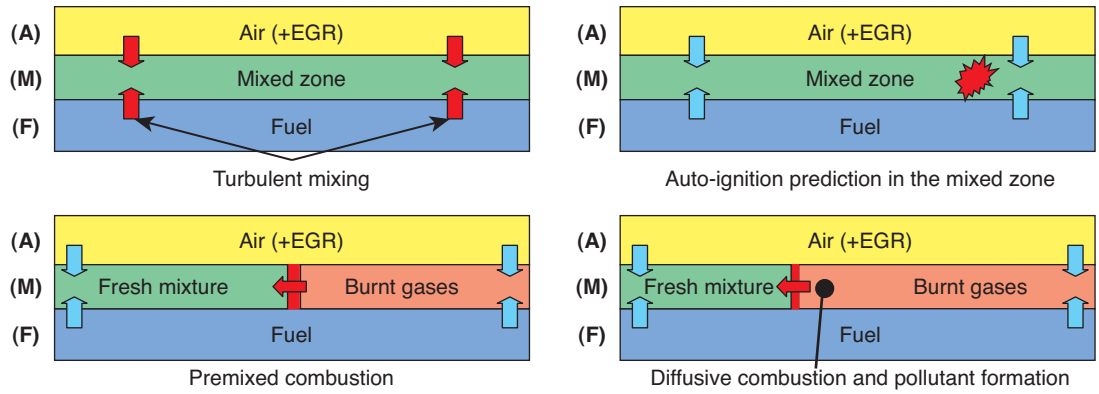


Figure 1

Description of the ECFM3Z model. Contribution of the different physical processes.

The air (+EGR)—fuel mixture may then auto-ignite in region M. Auto-ignition can be handled by various specific models which provide the auto-ignition delay that ECFM3Z integrates over time. When the auto-ignition delay is reached, combustion in the region M starts, thereby dividing it into two zones: an unburnt and a burnt gas zone. As the unburnt gases from the unburnt zone in region M are oxidised by auto-ignition, the formed hot products are added to the burnt gases zone in region M.

## 3 AUTO-IGNITION MODELLING

### 3.1 Context

In the context of 3D CFScombustion calculations, the auto-ignition process can essentially be seen as the rapid oxidation of a premixed charge of fuel and air. The modelling challenge is then to predict when and where this auto-ignition will take place. In internal combustion engines, auto-ignition can include cool flame (low temperature) chemistry, depending on local conditions.

This cool flame process is essential in all HCCI engines using early injection strategies or port fuel injection. Being a part of this HCCI family, precise CAI™ auto-ignition modelling is consequently related to the ability of the model to represent this phenomenon.

### 3.2 Overview of Auto-Ignition Modelling Strategies

Progress in engine design is motivated by the emergence of environmental regulations as underlined in the introduction of this work. The intensive use of numerical modelling is now seen as an essential stage both for physics understanding and predictive applications. Among the many processes involved in engine combustion modelling, auto-ignition is a major aspect because physics understanding is still under investigation and application demands are growing. This is one of the main reasons why combustion sub-models allowing for the introduction of complex and detailed chemistry, mostly via a tabulation of the subtle intermediate chemical paths controlling ignition, extinction, and pollutant emissions, have been flourishing in the literature for the past decade. Along these lines, and starting from the knowledge of fully detailed chemical schemes [22], various methodologies have been proposed to tabulate complex chemistry. One of them, ILDM (Intrinsic Low-Dimensional Manifold) [23], is based on a direct mathematical analysis of the dynamic behaviour of the non-linear response of the chemical system. Relevant subspaces are determined by distinguishing between chemical evolutions linked to fast and slow time scales. Other techniques, such as ISAT [24], are based on *in situ* generations of look-up tables, which are constructed "on the fly" from the direct solving of the time evolution of the species concentrations.

In most engine combustion problems featuring complex geometry, the large number of transported scalars involved in the detailed chemical mechanism needs to be highly reduced, for example, by using tabulations. To provide such tabulations, several similar methods based on *a priori* detailed chemistry calculations were recently proposed: the FPI (Flame Prolongation of ILDM) method [25], the FGM (Flamelet-Generated Manifold) [26] and the TKI method (Tabulated Kinetics of Ignition) [27]. The first two techniques are based on the tabulation of a set of unstrained premixed laminar flames. For a given equivalence ratio $\phi$ of the reactive mixture, FPI tabulates the chemical response of laminar flames from a progress variable $Y_c$, which varies from $Y_c^f(\phi)$ in fresh gases to $Y_c^b(\phi)$ in the burned gases. Then, any concentration, temperature or thermodynamic property can be uniquely related to the progress variable and the local equivalence ratio, $\phi = \phi(Z)$, sometimes expressed with the mixture fraction $Z$. Some extension of the FPI method was proposed to deal with auto-ignition [28]. In the following, we focus on an approach similar to FPI but which is originally dedicated to the auto-ignition process in internal combustion engines: the TKI model.

### 3.3 TKI: A Model Based on Reaction Rates

The Tabulated Kinetics of Ignition (TKI) auto-ignition model relies on tabulated auto-ignition parameters deduced from detailed chemistry calculations. These chemistry calculations are performed with the Senkin code [29] which is part of the Chemkin package [30].

The target is to correctly reproduce the temperature *vs* time evolution, like the one represented in Figure 2, for a set of operating conditions which matches the range of conditions that one may expect to meet in a CAI$^{TM}$ engine. These conditions are imposed by the technology (inlet gas temperature, injection strategy, valve lift and timing, EGR rates, etc.).

To build a convenient database, the appropriate thermodynamic conditions have to be chosen. To cover both standard spark-ignition (knocking modelling) and CAI$^{TM}$ operating points, the Senkin calculations at constant pressure are realised for the following sets of initial thermodynamic conditions:

- Temperature: 400 to 1500 K;
- Pressure: 0.1 to 8MPa;
- Fuel/air equivalence ratio: 0.3 to 3.0;
- Dilution gas fraction (Xres) relative to air: 0%, 30%, 60%, 80% and 90%;
- Octane Number* (IO): 50 to 100.

* The calculations are performed for Primary Reference Fuel (PRF) leading to identical Research Octane Number and Motor Octane Number. Consequently, the fuel is a mixture of n-heptane ($nC_7H_{16}$) and isooctane ($iC_8H_{18}$). Using this formalism for the fuel description, n-heptane stands as "PRF 0" and is used to model Diesel auto-ignition [18], [27], [31]. By this mean, the model proposed hereafter is a unified model which handles both gasoline and Diesel auto-ignition.

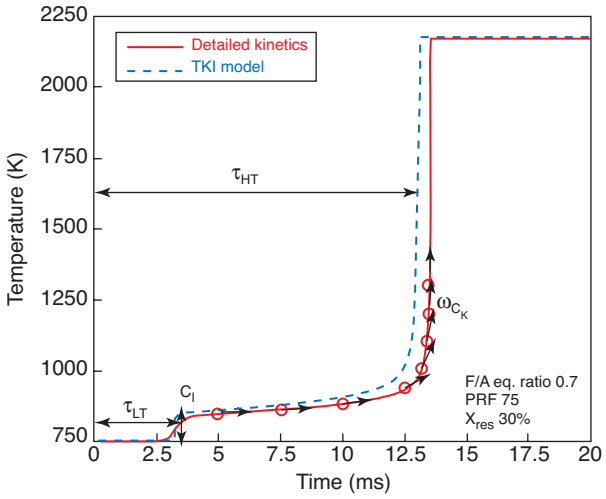


Figure 2

Comparison of the temperature *vs* time evolutions between detailed kinetics and the TKI model on a constant volume homogeneous case – $\phi = 0.7$, $X_{res} = 30\%$, IO = 75.

The initial molar composition for the detailed kinetics computation ($Xnc_7h_{16}$, $Xic_8h_{18}$, $Xo_2$, $X_D$ (where $X_D$ is the molar fraction of dilution gases) is determined as follows:

$$\begin{aligned} \phi &= \alpha \frac{X_{Fu}}{X_{O_2}} \quad with \quad \alpha = \frac{3}{2} IO_x + 11 \\ X_{Fu} &= (1 - IO_x) X_{nc_7h_{16}} + IO_x X_{ic_8h_{18}} \\ X_{res} &= 1 - \frac{4.76\, X_{O_2}}{X_{O_2} + X_D} \\ X_{Fu} &+ X_{O_2} + X_D = 1 \end{aligned} \tag{1}$$

In these expressions, $IO_x$ has a value between 0 and 1. It is the fraction of $iC_8H_{18}$ for one mole of the PRF mixture which octane number is $IO = 100\ IO_x$. One can note that, in this system, $X_{res}$ is seen as the amount of non-reactive species ($N_2$, $CO_2$, $H_2O$, Ar, etc.) in excess of the amount of $N_2$ present in air. In what follows, one needs to be careful that the definition adopted here matches the definition of $X_{res}$ used for experimental results.

#### 3.3.1 Complex Chemistry – 3D CFD Coupling Approach

The database generation algorithm is an automatic procedure executing the following operations successively (*Fig. 3*): the molar composition is computed (see previous section for details), an input file is written and the detailed chemistry calculation is run for each initial thermodynamic condition. The detailed mechanism of the n-heptane/iso-octane mixture is used for all the simulations. It is generated by the DCPR (Département de Chimie Physique des Réactions, CNRS, Nancy) following an automatic procedure described in [32] along fundamental elementary chemical rules. One obtains a 416 species 1992 reactions detailed mechanism. To avoid extra computational times in the database generation, the temperature discretisation step is enlarged at low initial temperatures (below 650 K) and high initial temperatures (above 1000 K) where the delays evolution is linear (see *Fig. 4*). Then, the temperature profiles obtained in these calculations are post-processed. After the relevant parameters of the 3D model are extracted from the database, the missing points in the low temperature and high temperature ranges are reconstructed by linear interpolation so that parameters are finally tabulated with a constant temperature step of 10 K in the 3D CFD code.

Then, the database construction is checked by plotting the delay evolutions as a function of 1000/T. The typical S-shaped curves obtained (see *Figure 4*) are used to identify irrelevant points.

Some points at very low F/A equivalence ratios, very high F/A equivalence ratios or high dilution rates may feature multiple inflexions on the temperature curve so that the target delay is not correctly post-processed. These points fail to be processed automatically and a specific manual treatment is applied. In order to cover the wide range of conditions

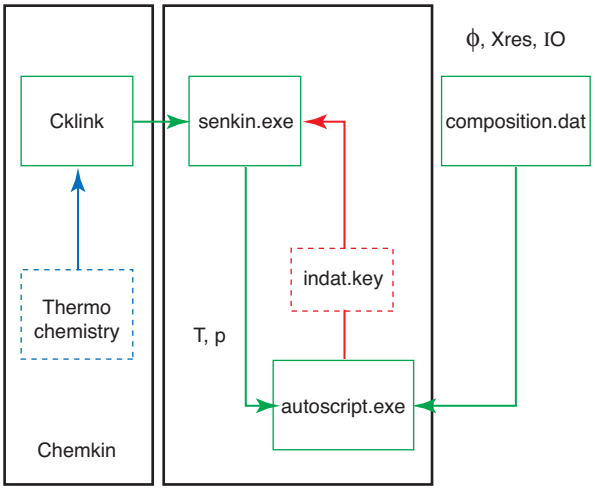


Figure 3

Automatic generation algorithm of a detailed chemistry database for a given composition and a range of temperatures and pressures. Files cklink, composition.dat are input data. File indat.key is updated for each initial temperature and pressure values and contains the molar fraction of each species as well as the numerical parameters related to the Senkin (senkin.exe) run.

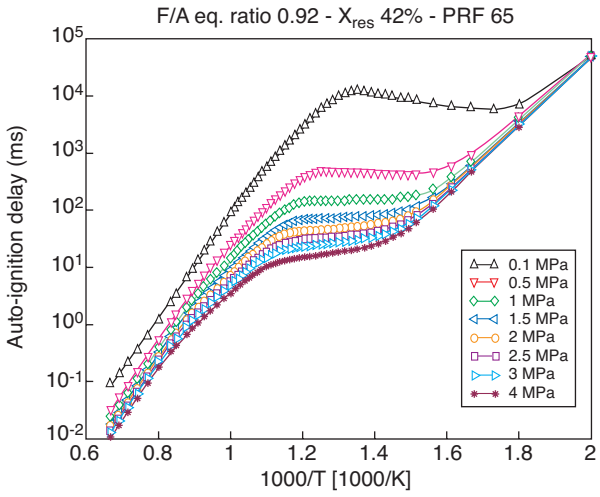


Figure 4

Delay evolution as a function of the temperature for various pressures

described above, including pure *n*-heptane for Diesel computations ("PRF 0"), 68400 Senkin calculations were performed. The 3D model parameters (see next sections) are calculated from this database once for all and stored in a table. This technique permits to dramatically save computational time compared to direct coupling between detailed chemistry and 3D thermodynamic as one may encounter in some models [21].

### 3.3.2 Cool flame equations

The delay curves plotted as a function of 1000/T represent the main ignition delay noted $\tau_{HT}$ (High Temperature). They feature typical S-shaped curves (*Fig. 4*) with an inflexion in the cool flame region, also called negative temperature region because the delays increase when the temperature increases. The lower and higher limits of this region vary with the thermodynamic conditions. It is essentially characterised by an early heat release at time $\tau_{LT}$ (Low Temperature) corresponding to a fraction $C_1$ of the total heat release as one can see in Figure 2. The precise modelling of this behaviour is the main task of the TKI model.

Like in [31], the cool flame delay is calculated through the integration of an intermediate species concentration $\tilde{Y}_I$ (the *tilde (~)* notation stands for the classical Favre average used in combustion modelling). Considering an homogeneous flow without convection and diffusion, the growth rate of $\tilde{Y}_I$ is proportional to the amount of the fuel tracer concentration $\tilde{Y}_{TFu}$ and to a function of the cool flame ignition delay defined earlier.

$$\frac{d\overline{\rho}\tilde{Y}_I}{dt} = \overline{\rho}\tilde{Y}_{TFu}F(\tau_{LT}) \tag{2}$$

The fuel tracer concentration $\tilde{Y}_{TFu}$ represents the amount of fuel in the mixing zone that would exist in the computational cell without chemical reactions. It is a passive scalar since it is neither consumed nor created by chemical reactions. The cool flame delay $\tau_{LT}$ comes from an interpolation inside the database as a function of local thermodynamic conditions in the computational cell. The term on the right hand side of Equation 2 represents the source term of the transport equation solved in the engine code for $\tilde{Y}_I$. From the definition of the intermediate species, the cool flame ignition delay in the computational cell is reached when the intermediate variable $\tilde{Y}_I$ is equal to the amount of fuel tracer present in the fresh gases.

When the cool flame delay $\tau_{LT}$ is reached, a portion of the fuel, denoted $C_1$, is consumed by the cool flame according to:

$$\frac{d\overline{\rho}\tilde{Y}_F}{dt} = -\overline{\rho}\frac{\tilde{Y}_F}{\tau_c} \tag{3}$$

This relation assumes that the cool flame chemistry is fast and the fuel consumption characteristic time $\tau_c$ is supposed to be constant. A reasonable hypothesis is to assume that $\tau_c$ is small compared to every other chemical times (including $\tau_{LT}$ and $\tau_{HT}$) so that the fuel is consumed almost instantaneously ($\tau_c = 2\ 10^{-6}$s). $C_1$ is extracted from the database through interpolation. In the absence of cool flame effect, $\tau_{LT} = \tau_{HT}$, $C_1 = 0$ and the reaction rate is computed according to the relations presented in the following section.

### 3.3.3 Main Ignition Equations

Main ignition is modelled on the basis of tabulated reaction rates as a function of a progress variable. This variable must therefore be defined. Since fuel in the 3D CFD code is burnt in a single step, the temperature rise is proportional to the amount of fuel consumed. The assumption is then made here that a progress variable based on fuel in the 3D CFD code is equivalent to a progress variable based on temperature in the detailed chemistry code [29].

This assumption, valid for an adiabatic incompressible flow with unit Lewis number, is acceptable in the framework of this model where the relevant information is the fuel consumption leading to a temperature increase. Problems would arise if other information such as species concentrations were to be extracted from the database. Consequently, the 3D CFD code reaction progress variable $\tilde{c}$ is defined as the ratio of the fuel consumed $\tilde{Y}_{TFu} - \tilde{Y}_{Fu}$ over the total vapour of fuel available $\tilde{Y}_{TFu}$ leading to:

$$\tilde{c} = 1 - \frac{\tilde{Y}_{Fu}}{\tilde{Y}_{TFu}} \tag{4}$$

After $\tau_{LT}$, while $\tilde{Y}_F \leq (1 - C_1)\tilde{Y}_{TF}$, the fuel consumption between the cool flame and the main ignition is a function of the progress variable reaction rate $\dot{\omega}_c$ and is calculated according to:

$$\frac{d\bar{\rho}\tilde{Y}_F}{dt} = -\bar{\rho}\dot{\omega}_c\tilde{Y}_{TFu} \tag{5}$$

The computation of $\dot{\omega}_c$ is based on the cell thermodynamic conditions ($T^u$, $p$, $\phi$, $X_{res}$, $IO$) leading to values $\dot{\omega}_{c_k}$ and $\dot{\omega}_{c_{k+1}}$ interpolated inside the database, where $\dot{\omega}_{c_k}$ is the reaction rate (time derivative of the progress variable $c$ based on the temperature profile) tabulated from detailed kinetics for progress variable $c_k$. The values of $c_k$ are discrete and have been chosen after several tests to represent correctly the main flame induction process after the cool flame delay has been reached. This has led to a set of seven values {0.025, 0.05, 0.075, 0.1, 0.15, 0.2, 0.3} which turned out to be a good compromise between the physics description ability and the size of the database. Figure 5 represents points of the database used to interpolate the parameters ($\tau_{LT}$, $C_1$, $\dot{\omega}_{c_k}$, $\dot{\omega}_{c_{k+1}}$) for a given set of conditions ($T^u$, $p$, $\phi$) assuming here for clarity that $X_{res}$ and $IO$ are kept constant.

### 3.3.4 Model Parameters Interpolation

The TKI model is integrated in the framework of the ECFM3Z model [16]. The fresh gases (or unburned gases) quantities ($T^u$, $p$, $\phi$, $X_{res}$, $IO$) are used as inlet parameters of the auto-ignition lookup tables. One needs to underline that the relevant temperature is the unburned gases temperature $T^u$ in the context of ECFM3Z according to the formalism described in [16]. The average octane number is computed locally as a function of the local fuel composition:

$$IO = \sum_j IO_j \tilde{X}_j \tag{6}$$

where $\tilde{X}_j$ is the molar fraction of fuel $j$ in the fresh gas state. A description of the interpolation procedure is presented in *Figure 5*. The model parameters are deduced from linear interpolation in the 5-dimension lookup tables for local conditions ($T^u$, $p$, $\phi$, $X_{res}$, $IO$) in the 3D CFD cells during computation.

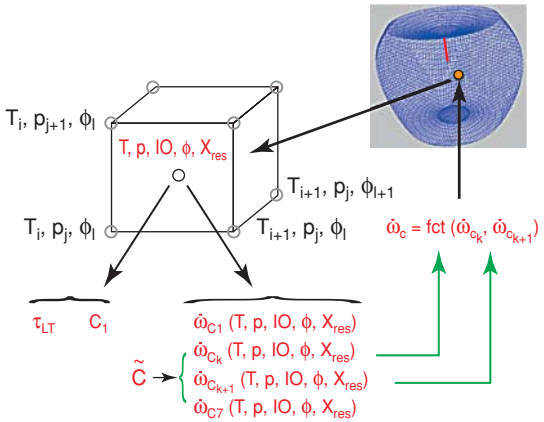


Figure 5

The cool flame heat release, the auto-ignition delay and the reaction rates are linearly interpolated for local thermodynamic conditions.

## 4 MODEL VALIDATION

### 4.1 Elementary Test Cases

To validate the model and the database integration several simple tests are performed. They consist in homogeneous calculations at constant volume performed with Senkin and with the TKI model. An example is presented in Figure 2 for $\phi = 0.7$, $X_{res} = 30\%$, IO = 75.

There is a good agreement in almost all cases provided that the initial conditions are inside the database. The cool flame delay and consumption integrated from the database are well-calculated as for the main ignition delay, computed by the reaction rates.

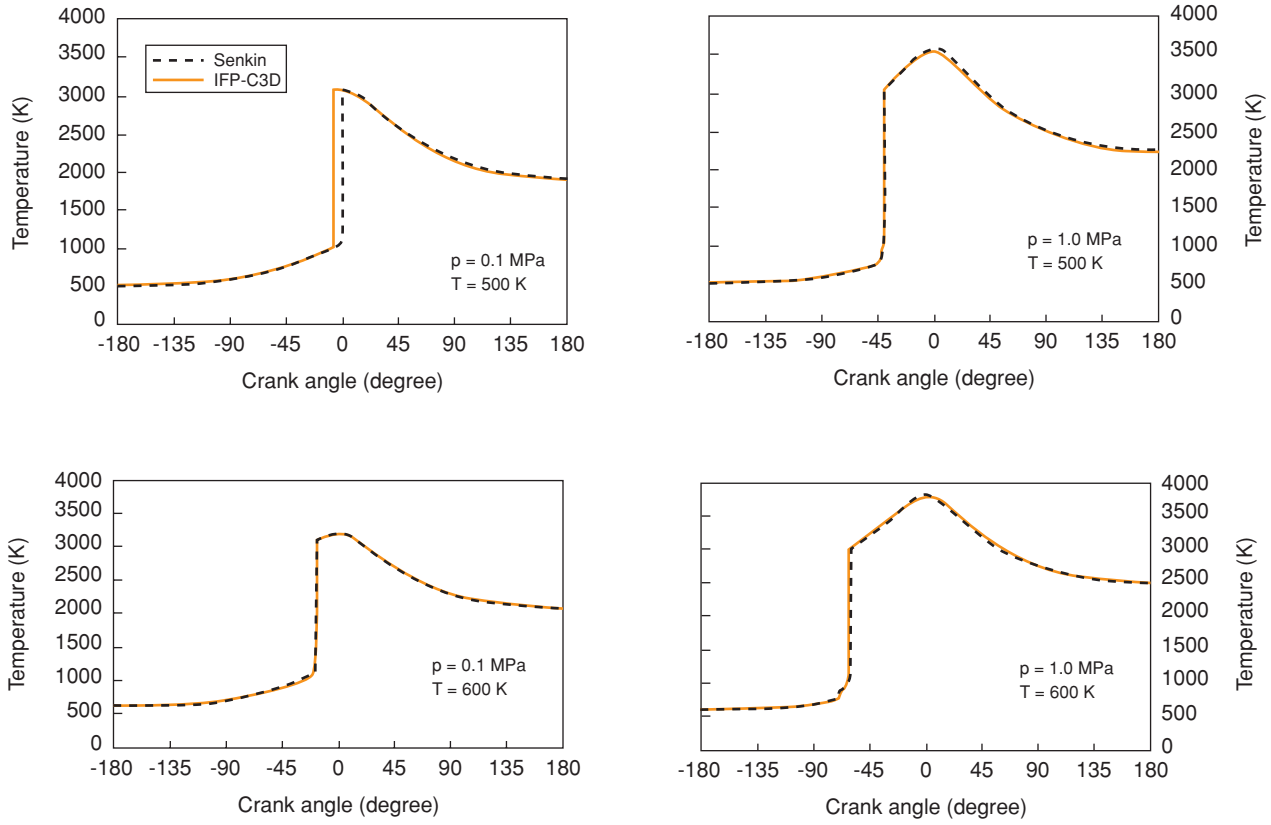


Figure 6

Comparison of Senkin and IFP-C3D results for various initial conditions.

As next validation step, simplified IC engine calculations are performed. To allow comparison with results from Senkin calculation, these are homogeneous calculations in an adiabatic engine for various initial conditions. A good agreement is obtained for conditions at compression BDC representative of CAI™ process (*Fig. 6*).

## 4.2 Rapid Compression Machine

The validations performed in this part consist of comparisons between delays computed with the proposed model and delays measured in a rapid compression machine. The experimental set up is described in [33]. It consists of an adiabatic compression machine (compression ratio is 9.6:1) following a specific piston motion law. The consequent volume evolution is the following:

$$V(t) = \begin{cases} 429.9 - 28.71t \text{ for } t \in [0; 2.58\,10^{-2}s] \\ 461.8 - 4.11t \text{ for } t \in [2.58\,10^{-2}s; 10.02\,10^{-2}s] \\ 76.01 - 2.605t \text{ for } t \in [10.02\,10^{-2}; 12\,10^{-2}s] \end{cases} \quad (7)$$

In the above expression, the volume is expressed in $cm^3$ and time in s. Dimensions of the chamber were calculated knowing the compression ratio and that the squish height and bore of this Rapid Compression Machine (RCM) are identical. One may deduce:

$$\begin{cases} \text{bore} = 3.85\,10^{-2}m \\ \text{stroke} = 33.12\,10^{-2}m \end{cases} \quad (8)$$

Thanks to this RCM [33], the auto-ignition delay is observed for different PRF (90 and 100) and several initial pressures as a function of the temperature at the end of compression and the Fuel/Air equivalence ratio. The variation in temperature at the end of compression is obtained by variation of the initial composition of the mixture: addition of carbon dioxide to decrease it and argon to increase it. The wall temperature, set at 373 K in all the experiments, is the initial temperature in the chamber. The Fuel/Air equivalence ratio of the mixture varies between 0.5 and 1.38 while keeping constant the temperature at the end of the compression (T = 690 K). The values obtained are compared with experimental results and with values computed previously using a single delay model [12] for a PRF 90 (*Fig. 7*).

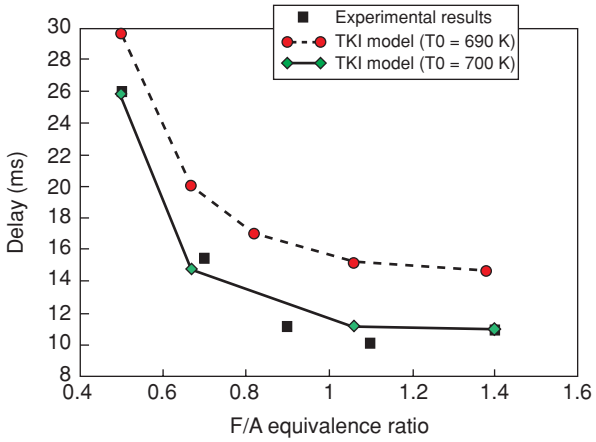


Figure 7

Influence of the fuel/air equivalence ratio on the auto-ignition delay measured on RCM. Comparisons between the measured delay (PRF 90) and the delay computed with the present model integrated in the IFP-C3D code.

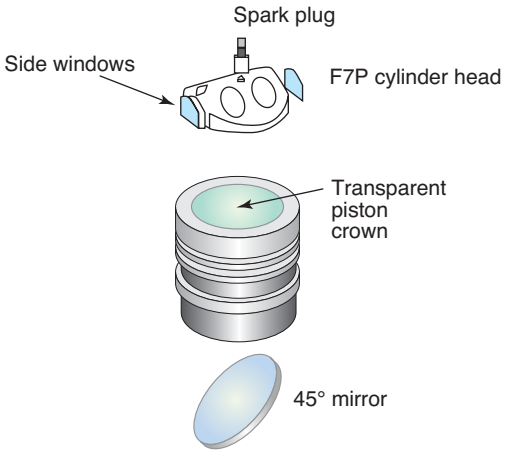


Figure 8

Engine optical accesses.

One may firstly note that the proposed model reproduces well the delay evolution as a function of the Fuel/Air equivalence ratio. The computed delays are globally larger than the measured delays. But we have to underline that the method used to compute the delay is based on the temperature maximum time derivative whereas the measured delay corresponds to the detection of the first spot of auto-ignition, which may explain the obtained overestimation.

Secondly, one may see the large sensitivity of the delay with the end of compression temperature. A temperature increase of about 10 K (1.5 %) results in a delay decrease of about 5 ms (25%). With a temperature of 700 K at the end of compression, one finds that the computed delays match perfectly the experimental delays.

Finally, we have to mention that this configuration is particularly interesting because the thermodynamic conditions (low local Fuel/Air equivalence ratios, low temperatures) are among the ones expected for CAI™ operating conditions.

## 5 EXPERIMENTAL SETUP AND OPERATING CONDITIONS

### 5.1 Single-Cylinder Engine

The modelled engine is a single-cylinder 4-stroke 4-valve pentroof engine with optical access based on a series Renault F7P. For the present study, Port Fuel Injection (PFI) is used with one injector in each intake pipe.

The optical accesses are two side windows in the cylinder head (which create additional dead volumes) and a transparent piston crown (see *Fig. 8*).

The main engine dimensions are summarised in Table 1. Note that the addition of the dead volumes for optical access and the increase of the compression ratio with respect to the series engine is obtained by a reduction of the distance between the piston and the cylinder head at Top Dead Center (TDC).

TABLE 1

Engine dimensions

| | |
|---|---|
| Bore x Stroke (mm) | 82.0 x 83.5 |
| Compression ratio (-) | 11.5:1 |

### 5.2 Valve Actuation Strategy

Two types of valve lift strategies are recognised as efficient to promote CAI™ combustion in a four-stroke engine [7]: the negative valve overlap strategy and the burnt gas re-breathing strategy.

The Negative Valve Overlap (NVO) strategy is design to only evacuate during the exhaust process the amount of burnt gases that would not be useful for heating up fresh mixture during the following cycle [10]. Therefore, the exhaust valve lift and timing are designed to obtain an early exhaust valve closure. For the remaining stroke of the piston to intake TDC, trapped burnt gases are recompressed. To avoid strong burnt gases backflow in the intake pipes, the intake valve opening has to be delayed till the expansion of in-cylinder gases produces pressure close to the intake one. At that time, the intake process may occur to provide the fresh mixture to auto-ignite. The main drawback of this valve strategy is the

recompression-expansion phase of the trapped burnt gases that, mainly due to heat transfer, produces pumping losses.

To override this drawback, the Burnt Gases Re-Breathing (BGRB) strategy has been designed. The idea is to allow a conventional exhaust process during the exhaust stroke and to force during the intake stroke simultaneous inlet of burnt gases (from exhaust pipes) and fresh mixture (from intake pipes). This strategy also induces its own drawback that is the loss of a part of the thermal potential of the exhaust gases. Indeed, the journey of the burnt gases in the exhaust pipes induces heat transfer that are more important than the ones encountered in the cylinder with the NVO strategy. Consequently, for an equal amount of burnt gases, the BGRB strategy will provide less heat potential to the fresh mixture of the following cycle but produces nearby no pumping loss.

As the NVO strategy is the easiest to apply to a conventional engine through the use of fully variable valve train (lift, duration and timing), this strategy is the most successful among the research engineers and is chosen for our reference operating point. The adapted valve lifts are shown in Figure 10.

### 5.3 Modelled operating point

The modelled operating point is a low load - low speed operating point: 0.29 MPa IMEP at 1200 rpm. This point has been chosen because it is a reference operating point for NVO strategy with a lot of available experimental data. Table 2 indicates the main characteristics of this operating point (experimental measurements).

TABLE 2

Operating conditions (experimental measurements)

| | |
|---|---|
| Engine speed (rpm) | 1200 |
| IMEP (MPa) | 0.29 |
| Air flow rate (g/s) | 1.586 |
| Vol. efficiency (-) | 0.30 |
| Intake F/A eq. ratio | 0.83 |

For optical diagnostic and CFD simulation, it is easier to use Primary Reference Fuel than commercial unleaded gasoline. But, to stay as close as possible to an industrial application, the PRF has to be carefully chosen to represent the behaviour of the commercial 95-octane unleaded gasoline. The experimental work realised at *IFP* showed that, for the present operating point, the PRF that best fits the results with commercial gasoline is the PRF 65 (35% n-heptane and 65% iso-octane) [7]. Consequently, the present calculation results are realised with a PRF 65 and compared with experimental measurements for this Primary Reference Fuel.

## 6 TEST BED MODELLING

To correctly simulate the experimental behaviour, the whole test bed equipment has to be modelled from the fresh air supplier to the exhaust gas extractor. As 3D CFD is limited to the combustion chamber and the intake and exhaust pipes (for the purpose of CPU time saving), 1D calculation is performed to provide precise boundary conditions.

The use of 1D CFD simulation results instead of directly measured experimental values has two main origins. First, the commonly measured values on test beds are either low frequency values (mean pressure, mean temperature, mean flow rate, etc.) or high frequency pressures. For 3D CFD calculation with inlet process (air intake or exhaust gas re-breathing), we have to provide two instantaneous thermodynamic parameters out of three possible: temperature, pressure and flow rate. The use of 1D simulation for the determination of the 3D CFD boundary conditions is consequently the best way to avoid erroneous approximation.

The second reason is the possibility to simulate, thanks to 1D CFD, operating points that are experimentally impossible to obtain because of technical limits (the experimental engine is an optical engine introducing limits in mechanical or thermal stress allowed) or very unstable behaviour (risk for costly equipment to be destroyed). Furthermore, once the 1D CFD model is considered reliable, it may be used to explore operating conditions that were never tested during experimental tests.

The 1D CFD model has been built with IFP-ENGINE in its first version integrated in AMESim platform V4.2.0. This 1D CFD library is developed at *IFP* and provides dedicated sub-models to simulate the behaviour of the engine and its immediate surroundings. The integration of this 1D CFD library on the same platform as the 3D CFD IFP-C3D code allows to easily exchange data between both levels of simulation.

The Figure 9 presents the sketch used for test bed modelling when the Port Fuel Injection set-up is considered. Two cylinder head sub-models are used in parallel for the only single-cylinder because there is a crank offset between the valve lifts, either for intake and exhaust valves.

The accuracy of the 1D model is tested by comparing its results with the experimental ones for the reference operating conditions. Figure 10 shows the intake pressure evolution at the location of the pressure sensor (limit of the 3D CFD mesh on the intake side). The Figure 11 depicts the mean in-cylinder pressure. As there is presently no predictive 1D model to represent CAI™ process, the combustion is described with a tuned Wiebe law. Finally, the Table 3 presents the mean engine results.

As such results are obtained with a description of the intake and exhaust paths directly deduced from the actual experimental elements, the 1D CFD model of the test bed is considered reliable. This model will consequently provide the needed boundary conditions for 3D CFD calculations.

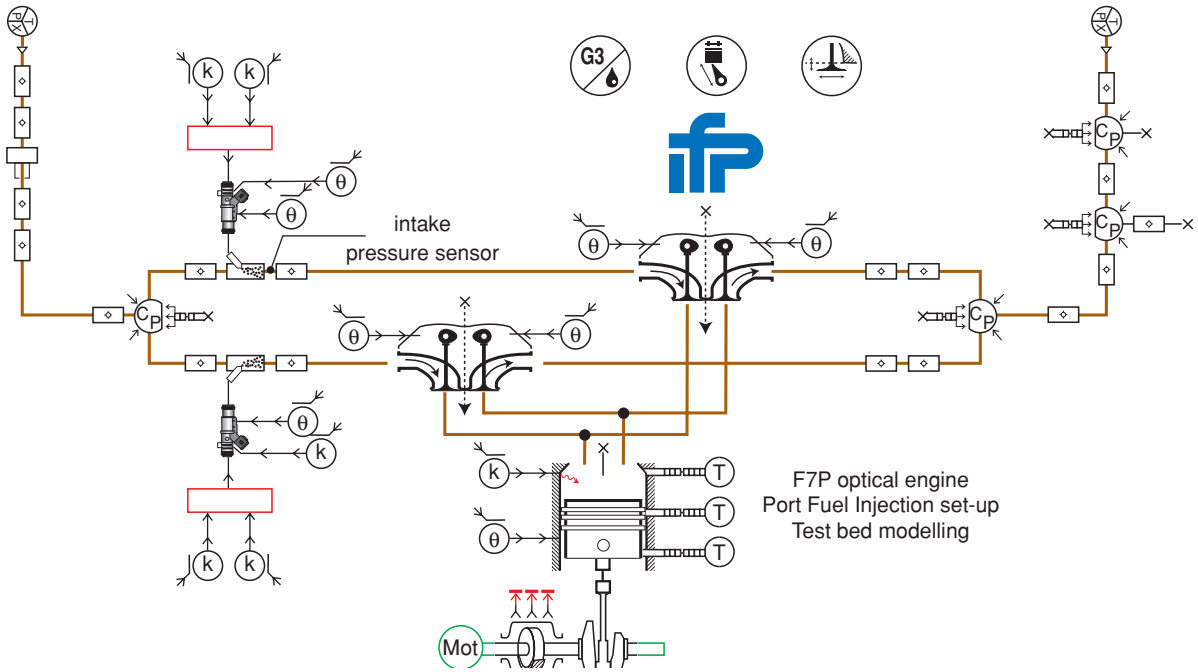


Figure 9

IFP-ENGINE sketch for the test bed modelling.

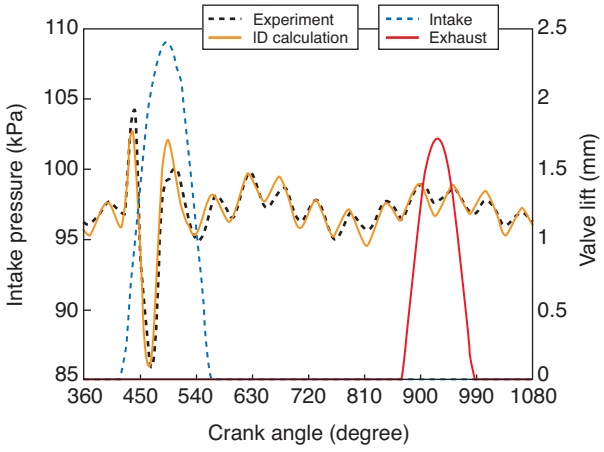


Figure 10

Intake pressure at the test bench pressure sensor.

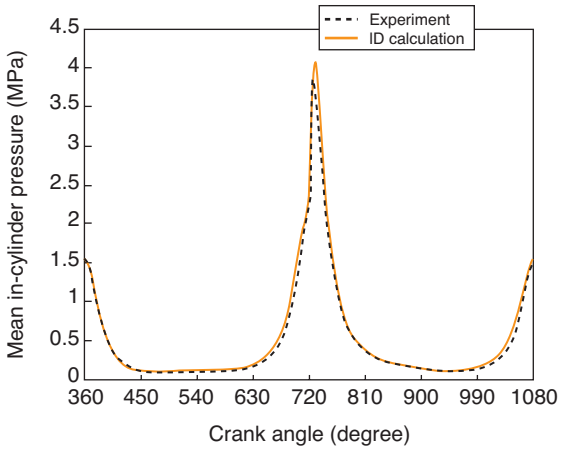


Figure 11

In-cylinder pressure trace.

TABLE 3

Low frequency data

| | Experiment | 1D Calculation |
|---|---|---|
| Air flow rate (g/s) | 1.586 | 1.605 |
| Intake F/A eq. ratio | 0.830 | 0.828 |
| IMEP (MPa) | 0.29 | 0.301 |
| EGR rate (%mass) | ? | 45.4 |

## 7 INTAKE PROCESS AND MIXTURE FORMATION

To provide exact initial conditions to combustion modelling, we do not only have to know the mean in-cylinder pressure, temperature or mass fraction for each species, but also the location of these species, the temperature field they induce or even the in-cylinder fluid motion. All the mean values should be provided by dedicated 1D CFD simulation but the in-cylinder fields have to be obtained through 3D CFD simulation.

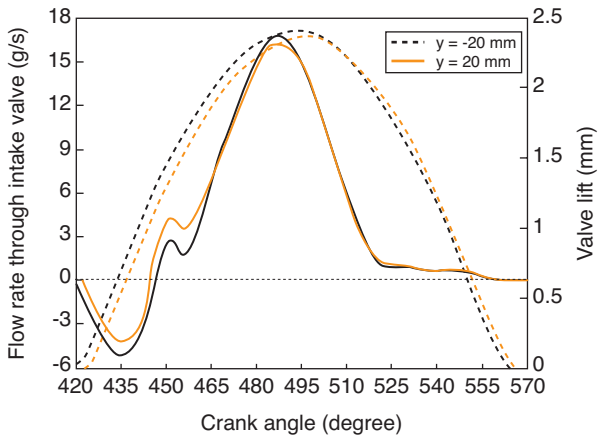


Figure 12

Intake flows through the intake valves (1D CFD results).

As the recompression phase (around intake TDC –360 cad) destroys most of the fluid motion existing at the end of the exhaust process, mean values are closed to real in-cylinder fields between intake TDC and the beginning of the intake process. So we choose to start the calculation at the beginning of the intake process with thermodynamic conditions provided by 1D CFD calculations. A full engine cycle is then calculated using 3D CFD to verify that these initial conditions are relevant.

## 7.1 Flow Through Intake Valves

Despite the late intake valve opening, there is backflow at the beginning of the intake process (see *Fig. 12*). Because the valve lifts are slightly offset, the earliest-opened intake port is more sensitive to the backflow. This is important for the in-port fluid motion and the consequent inlet efficiency of the port because the intake ports are fully separated in the cylinder head and way upstream since the intake manifold.

At the end of the intake process (around compression BDC –540 cad), the intake flow is nearby null despite the "relatively high" valve lift (around 2 mm for a maximal valve lift of around 2.4 mm). Consequently, there is around 25 cad of backflow and only around 75 cad of inflow. Besides, the first 20 cad of inflow are dedicated to the reaspiration of the "backflowed" burnt gases.

## 7.2 Mixture Formation

One of the main concerns about CAI™, as a part of the HCCI family, is how far the mixture is homogeneous. Precedent work at *IFP* and elsewhere [7, 11] demonstrated that the mixture is not perfectly homogeneous but also that no major heterogeneity is present for the most efficient operating points near combustion TDC. It thus seems that a subtle management of the heterogeneity induced by the scavenging strategy is one of the major key for the control of the CAI™ process.

### 7.2.1 Mixture During Intake Process

The use of low valve lifts to control the amounts of burnt and fresh gases produces unusual fluid motion (see *Fig. 13*). The highest fresh mixture momentum and consequent penetration is obtained in the symmetry plane of the combustion chamber. On the contrary, in the mid valve planes, the fresh mixture is kept very close to the valve. The motion of the fresh mixture in the symmetry plane is very directive implying to send the fresh mixture directly onto the piston below the exhaust valves. After the impact of the fresh mixture on the piston, a part of the fresh gases goes up along the cylinder liner below the exhaust valves but the main part moves along the piston towards the intake side creating a tumble motion. The global tumble motion is favourable to obtain an efficient mixture; this allows to bring the heat of the trapped burnt gases to the fresh ones.

At the beginning of the compression stroke, there is still a pocket of burnt gases along the cylinder liner below the intake valves (*Fig. 14*). During the compression (see next paragraph and *Fig. 16*), the tumble motion provides mixing but this pocket still exists (even if the heterogeneity intensity decreases) and is moved along the cylinder head to the exhaust valves. Consequently, near TDC, the intensity of the existing heterogeneities is low but a slight gradation is present with highest burnt gas rate below the exhaust valves.

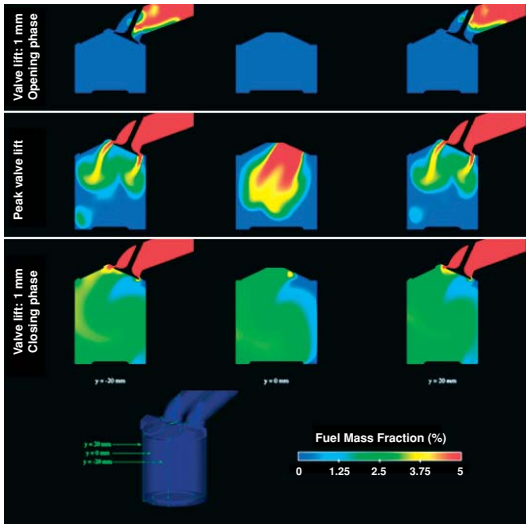


Figure 13

Fuel mass fraction field during the intake process (3D CFD calculation results).

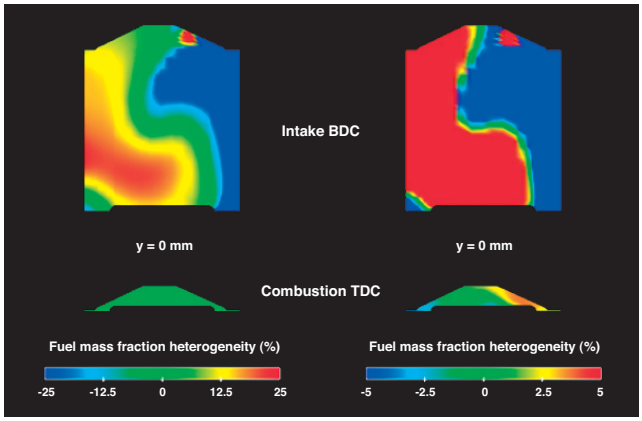


Figure 14

Degree of heterogeneity of the fuel mass fraction field (3D CFD calculation results).

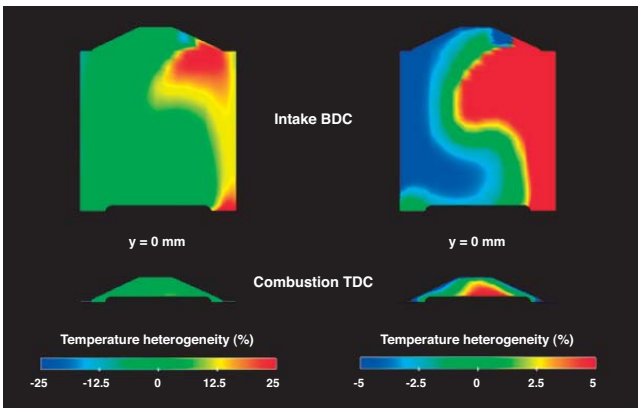


Figure 15

Degree of heterogeneity of the temperature field (3D CFD calculation results).

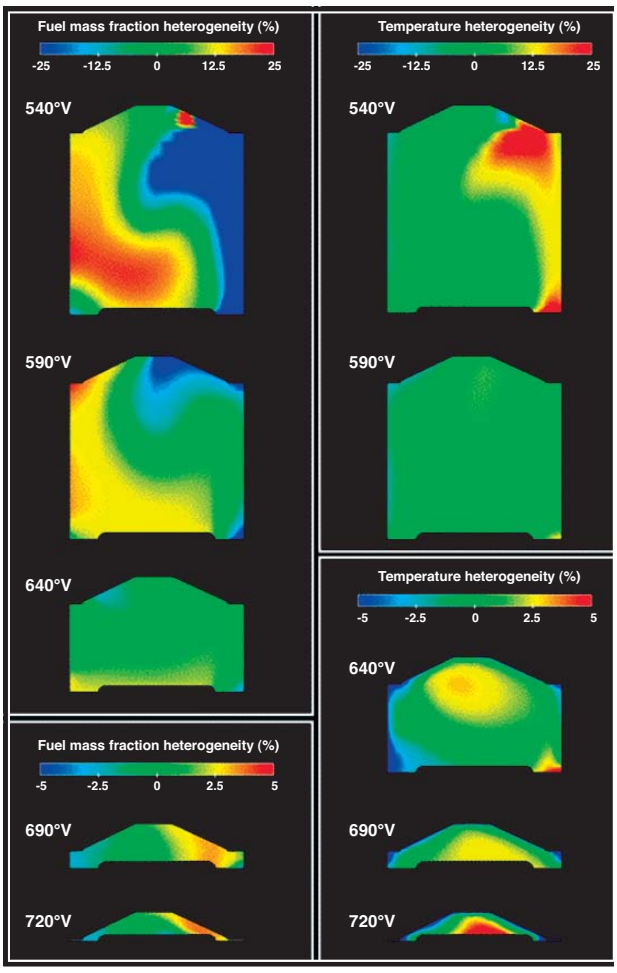


Figure 16

Evolution of the heterogeneity of fuel mass fraction and temperature (3D CFD calculation results).

### 7.2.2 Heterogeneity of the Mixture

To evaluate the degree of heterogeneity of the mixture for our reference operating point, there is no use of plotting absolute values because the evolution of these values is mainly due to the mean evolution of the value (for example, temperature or pressure). Consequently, the depicted fields are the relative gap of the value with its mean (calculated in the whole computational volume).

The evolution of the auto-ignition delays is depending on 5 parameters: the local temperature, the local pressure, the local dilution rate, the local Fuel/Air equivalence ratio and the local octane number. The octane number is depending on the fuel but no local variation may be obtained because the simulation is performed for a unique PRF (assuming a perfectly homogeneous mixture of n-heptane and iso-octane). Furthermore, before auto-ignition occurs, no major heterogeneity for pressure may be created. Consequently, there are only three relevant parameters: temperature, dilution and F/A eq. ratio.

The reference operating point is a PFI operating point and the injection process in the intake pipe is not simulated. As a consequence, the mixture of fuel and air is supposed perfect in fresh mixture. But the fresh mixture being lean, there is oxygen in the exhaust gases and, consequently, the local F/A eq. ratio is a direct inverse function of the dilution, reducing the number of relevant parameters to two (local dilution and F/A eq. ratio are linked).

The intensity of the heterogeneity for all values is varying with the advancement of the intake and compression processes. The heterogeneity is naturally very important at the beginning of the intake process and diminishes as the induced fluid motion promotes mixing. To have at our disposal exploitable views, two heterogeneity scales are used: +/–25% and +/–5%. The +/–25% scale is chosen because it is

approximately the sensitivity of the optical diagnostic techniques that indicate homogeneous mixture near combustion TDC. The +/-5% scale is the best adapted for visualisation near combustion TDC.

The observed fields are the intensity of the heterogeneity of the local temperature and fuel mass fraction (directly linked to F/A eq. ratio and dilution). At the beginning of the intake process, the temperature field is the negative of the fuel field as there is only fuel in the fresh mixture and the trapped burnt gases is the main heat source. The heat losses and heat diffusion are the origin of the diverging evolution of these fields during the intake and compression processes (*Fig. 16*).

Figure 14 and Figure 15 indicate the intensity of the heterogeneity during the compression. At compression BDC, the most relevant scale is the +/–25% scale which means that there is a difference of around 50% of the mean value between the lowest and highest local values. On the contrary, at combustion TDC, the relevant scale is +/–5% what is the explanation for the appearant homogeneity observed during optical diagnostic visualisation (used optical diagnostic techniques have sensitivity around +/-25%).

These heterogeneity fields show that the homogeneity is not absolute. At combustion TDC, in the symmetry plane of the chamber, the fuel mass fraction is higher below the intake valve. As a higher local Fuel/Air equivalence ratio is favourable to lower the auto-ignition delay, the auto-ignition should appear first below the intake valves. For the temperature field, the importance of the heat losses near the piston (due to a very reduced squish height) imposes the highest local temperature in the centre of the chamber. As a consequence, the area below the intake valve on the side of the valve facing the exhaust valve should be the most favourable auto-ignition area (assuming that no cool flame is present as observed during experimental tests and present calculation results – see next section).

## 8 AUTO-IGNITION AND COMBUSTION EVOLUTION

As shown in Figure 17, the first auto-ignition site is located below one of the intake valves, the one that is opened first during the intake process. The location of the auto-ignition site below one of the intake valves has been explained in the preceding paragraph. The difference between both intake valves is due to an heterogeneity of lower intensity in the plane parallel to the piston that produces slightly more favourable conditions below the earliest-opened valve.

As the conditions for auto-ignition are more favourable below the intake valves, it is natural that the heat released by the first auto-ignition site quickly induces auto-ignition in the neighbouring area below the other intake valve. On the contrary, the extension of the burning area towards the exhaust valves is largely delayed. This evolution in the location of the burning areas is the one observed during experimental tests [7].

In Figure 17, the red and blue iso-surfaces indicate the limits of the burning zones. The red iso-surface is the location of the local auto-ignition occurrence. The blue iso-surface indicates the area where combustion is not possible anymore because all the locally available fuel has been oxidised. In the whole combustion chamber, the fuel oxidation is so quick that any site where auto-ignition occurs burns all the available fuel. The zones where there is still fuel at the end of the combustion process are simply zones where auto-ignition never occurs.

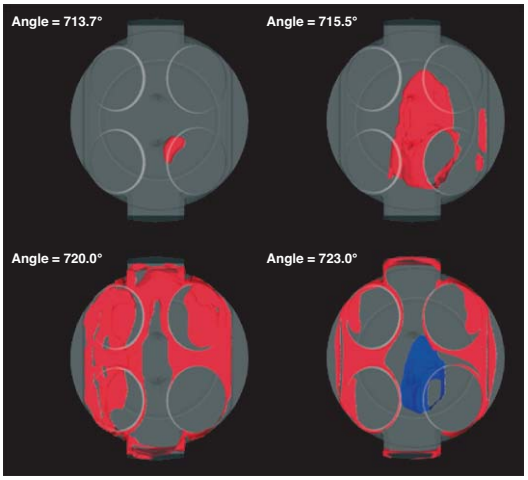


Figure 17

Evolution of combustion location (3D CFD calculation results).

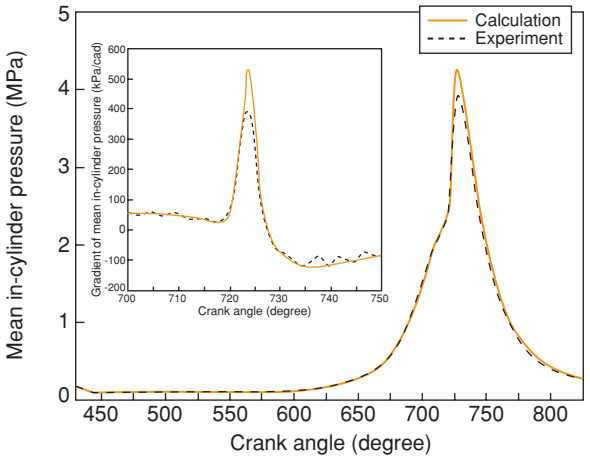


Figure 18

Evolution of mean in-cylinder pressure and pressure gradient.

It is important to note that the auto-ignition is obtained through the occurrence of main flame auto-ignition. Indeed, nowhere cool flame auto-ignition could be detected for the present operating point. This behaviour is also noted during engine operation [7] where the specific light emission of the cool flame is never registered when visualising the combustion.

Another important information is the way the combustion progresses: there is no front flame moving in the combustion chamber (depicted surfaces in *Fig. 17* are not front flame, they are just iso-surfaces of equal reaction rate). The evolution of the combustion through the chamber is only due to the local increase of temperature due to neighbouring combustion. This increase in temperature allows to reach propitious conditions for the auto-ignition. This way of propagation of the combustion is the reason why the non-burning areas are all near-wall zones. Indeed, because of the high heat losses in these zones, the local temperature never increases sufficiently to promote auto-ignition.

The location of the auto-ignition sites and the propagation of the combustion are in good agreement with the visualisations in the optical engine. The fact that combustion ends at the earliest auto-ignition sites when the latest are just starting to burn has also been observed experimentally. It is a consequence of the rapid oxidation mechanisms controlling the combustion that have a shorter time scale than heat diffusion through the chamber.

As can be seen in Figure 18, the timing of the numerical combustion is in quite good agreement with the experimental results even if a slight delay exists (see *Fig. 20*). Nevertheless, the peak in-cylinder pressure (and consequently the in-cylinder pressure during the first part of the expansion) is overestimated.

Previous optical diagnostic research work [7] highlights a link between the location of the earliest auto-ignition sites and the slightly fuel richer zones. For local burnt gas rate, no influence on the location of the auto-ignition sites was detected because the sensitivity of the measurement leads to the observation of a homogenous field for burnt gas rate.

To compare these experimental observations with our present simulation results, the location of 3 iso-surfaces is plotted (*Fig. 19*) to be compared with the location of the first auto-ignition site (*Fig. 17*). The red iso-surface represents the highest local temperature; its location is precisely the location of the first auto-ignition site which is coherent with the occurrence of main flame auto-ignition and outlines the predominant influence of local temperature. The blue iso-surface indicates the lowest local burnt gas rates; its location is also very close to the one of the first auto-ignition site. It is very interesting to note that despite low local burnt gas rate, high temperature is obtained. The influence of these two parameters on auto-ignition is clear: the higher the local temperature, the shorter the auto-ignition delay; and the lower the local burnt gas fraction, the shorter the auto-ignition delay.

Finally, the green iso-surface shows the higher local Fuel/Air equivalence ratio. As for both other parameters, the local value near the auto-ignition site is the most favourable to the auto-ignition occurrence (the higher the local Fuel/Air equivalence ratio – for lean mixtures –, the shorter the auto-ignition delay). But, contrary to both other parameters, the same local value is also existing in other not-igniting zones, indicating that this parameters is probably not a first order parameter. Comparing these results with experimental observations, we may note that the link between the highest local Fuel/Air equivalence ratio and the first auto-ignition site is a common conclusion [7]. But, on the other hand, this link

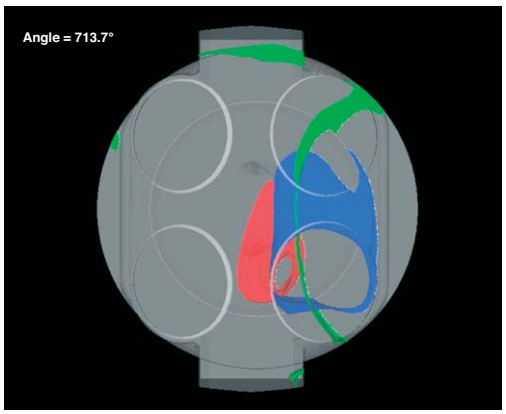


Figure 19

Location of high temperature (red), high Fuel/Air equivalence ratio (green) and low burnt gas rate (blue) (3D CFD calculation results).

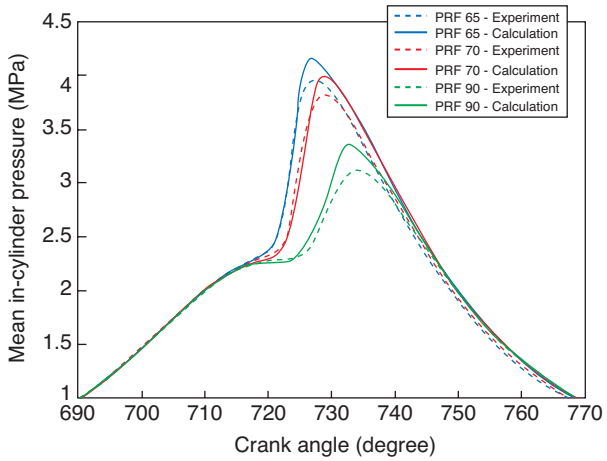


Figure 20

Influence of the PRF on the auto-ignition timing.

seems to be less influential than the link between local temperature and the first auto-ignition site location.

## 9 SENSITIVITY TO THE PRF

As indicated previously, the Primary Reference Fuel whose behaviour best fits the one of commercial 95-octane unleaded gasoline is the PRF 65 (35% of n-heptane and 65% of iso-octane). To define the best fitting PRF, measurements have been experimentally realised for various PRF's. As the octane number is one of the main parameters for auto-ignition modelling, the sensitivity of the model to this parameter has to be tested. That for, the measurements obtained for other PRF's are used.

Figure 20 compares the calculation results with the experimental measurements for PRF 65, PRF 70 and PRF 90. One may notice that the difference in auto-ignition timing between the two PRF's is well reproduced even if the overestimation of peak in-cylinder pressure is still present.

The auto-ignition model appears to be reliable when considering variations in PRF composition (more iso-octane induces later combustion). Let us call back to reader's mind that a Primary Reference Fuel has identical Research Octane Number and Motor Octane Number but also that experiment demonstrated that the octane number testing methods are unable to provide a representative classification of fuels in CAI™ operating conditions. Consequently, an additional model is needed to link (depending on local conditions) a commercial 95-octane unleaded gasoline with PRF 95 in octane number testing methods and PRF65 in CAI™ operating conditions.

## CONCLUSION

An existing auto-ignition model developed at *IFP* for Diesel fuel and knocking conditions with gasoline has successfully been extended to gasoline HCCI operating conditions and more specifically validated for CAI™ operating conditions.

The TKI model for auto-ignition prediction and subsequent fuel consumption is based on the tabulation of various parameters describing the auto-ignition occurrence and timing and the evolution of chemical processes. The tabulated database is deduced from detailed chemistry computational results for a wide range of initial thermodynamic conditions, octane numbers and dilution rates. An automatic procedure to perform and to analyse the detailed chemistry calculations has been created to allow a rapid database update when the thermodynamic conditions are extended or a new chemical mechanism is available.

The validity of the model has been tested for simple test cases and full 3D CFD calculations on an optical engine using CAI™ combustion process. For CAI™ modelling, the results provided by the model are in quite good agreement with the experimental measurements, not only for mean in-cylinder pressure, but also for first auto-ignition site location and combustion evolution through the chamber. These 3D CFD results provide indications on the homogeneity of the mixture in a CAI™ engine and its influence on the auto-ignition sites location.

Future work with this new auto-ignition model will be devoted to the explanation of the limits of the CAI™ operating range and the research of new means for its extension. Various injection and valve lift strategies have already been experimentally demonstrated as efficient for CAI™ operating range extension, but the nature of their efficiency is still unknown. The information provided by the present new auto-ignition model is expected to be a source for further steps in the understanding of the chemical and mixture processes controlling these strategies.

## ACKNOWLEDGEMENT

The authors would like to thank S. Friederich for his valuable involvement in the 3D CFD calculation process.

## BIBLIOGRAPHY

1 Haraldsson G., Tunestål P., Johansson B. and Hyvönen J. (2002) HCCI combustion phasing in a multi-cylinder engine using Variable Compression Ratio. *SAE paper 2002-01-2858, Powertrain & Fluid Systems Conference & Exhibition,* San Diego, California USA, October 21-24.

2 Hyvönen J., Haraldsson G. and Johansson B. (2003) Operating range in a multi-cylinder HCCI engine using Variable Compression Ratio. S*AE paper 2003-01-1829, 2003 JSAE/SAE International Spring Fuel & Lubricants Meeting,* Yokohama, Japan, May 19-22.

3 Martinez-Frias J., Aceves S.M., Flowers D., Smith J.R. and Dibble R. (2000) HCCI engine control by thermal management. *SAE paper 2000-01-2869, International Fall Fuels and Lubricants Meeting and Exposition,* Baltimore, Maryland, October 16-19.

4 Hiraya K., Hasegawa K., Urushihara T., Iiyama A. and Itoh T. (2002) A study on gasoline fueled compression ignition engine "a trial of operation region expansion". *SAE paper 2002-01-0416, SAE 2002 World Congress,* Detroit, Michigan, March 4-7.

5 Lavy J., Dabadie J.C., Angelberger C., Duret P., Willand J., Juretzka A., Schäflein J., Ma T., Lendresse Y., Satre A., Schulz C., Krämer H., Zhao H. and Damiano L. (2000) Innovative ultra-low $NO_x$ Controlled Auto-Ignition combustion process for gasoline engines: the 4-SPACE project. *SAE paper 2000-01-1837, International Spring Fuels & Lubricants Meeting & Exposition,* Paris, France, June 19-22.

6 Graf N., Gronki J., Schulz C., Baritaud T., Cherel J., Duret P. and Lavy J. (2001) In-cylinder combustion visualization in an auto-igniting gasoline engine using fuel tracer- and formaldehyde-LIF imaging. *SAE paper 2001-01-1924, International Spring Fuels & Lubricants Meeting & Exhibition,* Orlando, Florida, May 7-9, 2001.

7 Thirouard B., Cherel J. and Knop V. (2005) Investigation of mixture quality effect on CAI combustion. *SAE paper 2005-01-0141, 2005 SAE World Congress*, Detroit, Michigan, April 11-14.

8 Lavy J., Dabadie J.-C., Duret P., Angelberger C., Le Coz J.F. and Cherel J. (2001) Controlled Auto-Ignition (CAI): A new highly efficient and near-zero $NO_x$ emissions combustion process for gasoline engine application. *A new generation of engine combustion processes for the future?*, 101-114, Editions Technip, Paris, France

9 Li J., Zhao H., Ladommatos N. and Ma T. (2001) Research and development of Controlled Auto-Ignition (CAI) combustion in a 4-stroke multi-cylinder gasoline engine. *SAE paper 2001-01-3608, International Fall Fuels and Lubricants Meeting and Exposition,* San Antonio, Texas, September 24-27.

10 Zhao H., Li J., Ma T. and Ladommatos N. (2002) Performance and analysis of a 4-stroke multi-cylinder gasoline engine with CAI combustion. *SAE paper 2002-01-0420, SAE 2002 World Congress,* Detroit, Michigan, March 4-7.

11 Cao L., Zhao H., Jiang X. and Kalian N. (2005) Numerical study of effects of fuel injection timings on CAI/HCCI combustion in a four-stroke GDI engine. April 11-14.

12 Lafossas F.A., Castagne M., Dumas J. P. and Henriot S. (2002) Development and validation of a knock model in Spark Ignition engines using a CFD code. *SAE paper 2002-01-2701, Powertrain & Fluid Systems Conference & Exhibition,* San Diego, California USA, October 21-24.

13 Kleemann A.P., Menegazzi P., Henriot S. and Marchal A. (2003) Numerical study on knock for an SI engine by thermally coupling combustion chamber and cooling circuit simulations. *SAE paper 2003-01-0563, 2003 SAE World Congress,* Detroit, Michigan, March 3-6.

14 Nishiwaki K., Yoshihara Y. and Saijyo K. (2000) Numerical analysis of the location of knock initiation in S. I. engines. *SAE paper 2000-01-1897, International Spring Fuels & Lubricants Meeting & Exposition,* Paris, France, June 19-22.

15 Zolver M., Klahr D., Bohbot J., Laget O. and Torres A. (2003) Reactive CFD in engines with a new unstructured parallel solver. *Oil & Gas Science and Technology,* n° 58, **1**, 33-46.

16 Colin O. and Benkenida A. (2004) The 3-zones extended coherent flame model (ECFM3Z) for computing premixed/diffusion combustion. *Oil & Gas Science and Technology*, n° 59, **6**, 593-609.

17 Colin O., Benkenida A. and Angelberger C. (2003) 3D modelling of mixing, ignition and combustion phenomena in highly stratified gasoline engines. *Oil & Gas Science and Technology,* n° 58, **1,** 47-62.

18 Réveille B., Miche M., Jay S. and Henriot S. (2004) Contribution of 3D CFD tools to the development and understanding of Diesel engines: improving today's engines and designing tomorrow's power units. *SIA International Congress*, Lyon.

19 Kleemann A., Laget O. and Jay S. (2005) CFD-Integrated Gasoline Development. *SIA International Congress*, Lyon.

20 Laget O., Kleemann A., Jay S., Réveillé B. and Henriot S. (2005) Gasoline Engine Development using CFD. *SAE paper to be published,* San Antonio.

21 Kraft M., Maigaard P., Mauss F., Christensen M. and Johansson B (2000) Homogeneous Charge Compression Ignition Engine: A simulation study on the effect of inhomogeneities. *ASME Technical Conference* Paper No. 2000-ICE-275, ICE, **34-2,** 63-70.

22 Lindstedt L. (1998) Modelling of the Chemical Complexities of Flames. *Proc. Combust. Inst.,* **27**, 269-285.

23 Maas U. and Pope S. (1992) Simplifying Chemical Kinetics: Intrinsic Low-Dimensional Manifolds in Composition Space. *Combust. Flame,* **88**, 239-264.

24 Pope S.B. (1997) Computationally Efficient Implementation of Combustion Chemistry Using In Situ Adaptive Tabulation. *Combust. Theory Modelling*, **1**, 41-63.

25 Gicquel O., Darabiha N. and Thévenin D. (2000) Laminar premixed hydrogen/air counterflow flame simulations using flame prolongation of ILDM with differential diffusion. *Proc. Combust. Inst.,* **28**, 1901-1908.

26 Van Oijen J.A., Lammers F.A. and de Goey L.P.H. (2001) Modelling of complex premixed burner systems by using flamelet-generated manifolds. *Combust. Flame,* **127**, 2124-2134.

27 Colin O., Pires da Cruz A. and Jay S. (2005) Detailed chemistry-based auto-ignition model including low temperature phenomena applied to 3-D engine calculations. *Proc. Combust. Inst.,* **30**, 2649-2656.

28 Embouazza M., Gicquel O. and Darabiha N. (2003) Modelling Auto-ignition of HCCI engine by reduced tabulated chemistry. *3rd Mediterranean Combustion Symposium*, Marrakech.

29 Lutz A., Kee R. and Miller J. (1987) Senkin: A Fortran program for predicting homogeneous gas phase chemical kinetics with sensitivity analysis. *Report No. SAND87-8248.UC-4, Sandia National Laboratory*.

30 Kee R., Rupley F.M. and Miller J.A. (1989) Chemkin II. A Fortran chemical kinetics package for the analysis of gas phase chemical kinetics. *Sandia Laboratories Report, SAND 89-8009B*.

31 Pires da Cruz A. (2004) Three-dimensional modelling of self-ignition in HCCI and conventional Diesel engines. *Combust. Sci. And Tech.,* **176**, 867-887.

32 Fournet R., Warth V., Glaude P.A., Battin-Leclerc F. and Scacchi G. (2000) Automatic reduction of detailed mechanisms of combustion of Alkanes by Chemical Lumping. *Int. J. Chem. Kinet.*, **32**, 36-51.

33 Halstead M.P., Kirsch J.L., Prothero A. and Quinn C.P. (1977) The auto-ignition of hydrocarbon fuels at high temperatures and pressures – fitting of a mathematical model. *Combust. Flame,* **30**, 45-60.


*Final manuscript received in December 2005*